

Exploiting CP-asymmetries in rare charm decays

Rigo Bause,^{*} Hector Gisbert,[†] Marcel Golz,[‡] and Gudrun Hiller[§]
Fakultät für Physik, TU Dortmund, Otto-Hahn-Str. 4, D-44221 Dortmund, Germany

We analyze patterns from CP-violating new physics (NP) in hadronic and semileptonic rare charm $|\Delta c| = |\Delta u| = 1$ transitions. Observation of direct CP-violation in hadronic decays, as in ΔA_{CP} , provides opportunities for $c \rightarrow u \ell^+ \ell^-$, $\ell = e, \mu$ transitions, and vice versa. For the concrete case of flavorful, anomaly-free Z' -models a NP-interpretation of ΔA_{CP} suggests measurable CP-asymmetries in semileptonic decays such as $D \rightarrow \pi \ell^+ \ell^-$ or $D \rightarrow \pi \pi \ell^+ \ell^-$. Conversely, an observation of CP-violation in $c \rightarrow u e^+ e^-$ or $c \rightarrow u \mu^+ \mu^-$ decays supports a NP-interpretation of ΔA_{CP} . Flavorful $U(1)'$ -extensions provide explicit U-spin and isospin breaking which can be probed in patterns of hadronic decays of charm mesons. We work out signatures for CP-asymmetries in $D^0 \rightarrow \pi^+ \pi^-$, $D^0 \rightarrow K^+ K^-$ and $D^0 \rightarrow \pi^0 \pi^0$, $D^+ \rightarrow \pi^+ \pi^0$ decays, which can be probed in the future at LHCb and Belle II and provide further informative cross checks.

I. INTRODUCTION

Suppressions of standard model (SM) amplitudes due to accidental symmetries provide useful directions for searches for new physics (NP). Among the salient features of $|\Delta c| = |\Delta u| = 1$ transitions within the SM are a strong Glashow-Iliopoulos-Maiani (GIM)-suppression and small CP-violation. Hierarchies of the Cabibbo-Kobayashi-Maskawa (CKM) matrix V suggest SM CP-violation at the order of $\text{Im}(V_{cb}^* V_{ub} / (V_{cs}^* V_{us})) \sim 7 \cdot 10^{-4}$, somewhat below LHCb's observation of CP-violation in charm [1]

$$\begin{aligned} \Delta A_{\text{CP}} &= A_{\text{CP}}(K^+ K^-) - A_{\text{CP}}(\pi^+ \pi^-) \\ &= (-15.4 \pm 2.9) \cdot 10^{-4}, \end{aligned} \quad (1)$$

where

$$A_{\text{CP}}(f) = \frac{\Gamma(D^0 \rightarrow f) - \Gamma(\bar{D}^0 \rightarrow f)}{\Gamma(D^0 \rightarrow f) + \Gamma(\bar{D}^0 \rightarrow f)}, \quad (2)$$

and the corresponding world average [2]

$$\Delta A_{\text{CP}}^{\text{HFLAV}} = (-16.4 \pm 2.8) \cdot 10^{-4}. \quad (3)$$

While this leaves room for NP, due to the sizable uncertainties of hadronic D -decays, Eqs. (1) and (3) provide no clear-cut sign of NP. On the other hand, ΔA_{CP} as large as the permille level is non-trivial to achieve in concrete models of NP. Correlations with other observables in charm and the down-quark sector exist, which are subject to partly very strong flavor constraints. For recent works, see Refs. [3–12]. Turning this around, the study of patterns using different sectors can hence disfavor or support a particular ΔA_{CP} interpretation, and vice versa.

In this work we pursue a global analysis of CP-asymmetries in rare hadronic and semileptonic charm decays. Our focus is on NP patterns induced by four-fermion operators. Links via dipole operators between hadronic and semileptonic CP-asymmetries in $D \rightarrow \pi \ell^+ \ell^-$ decays have been pointed out by Ref. [13]. We work out predictions and correlations for anomaly-free Z' -extensions of the SM with generation-dependent $U(1)'$ -charges, see Refs. [14–20] for recent phenomenological works. Flavorful charges can give rise to explicit isospin and U-spin breaking effects. It is our goal to work out corresponding experimental signatures for hadronic charm decays, exploiting yet another SM null test strategy in charm [21].

This paper is organized as follows: In Section II we briefly review CP-violation in hadronic D -decays, D -mixing and semileptonic $c \rightarrow u \ell^+ \ell^-$ transitions. In Section III we analyze effects of anomaly-free $U(1)'$ -extensions with generation-dependent charges in hadronic 2-body D -decays and how D -mixing constraints can be evaded to address ΔA_{CP} . Patterns among CP-asymmetries in $D^0 \rightarrow \pi^+ \pi^-$, $D^0 \rightarrow K^+ K^-$, $D^0 \rightarrow \pi^0 \pi^0$ and $D^+ \rightarrow \pi^+ \pi^0$ decays are worked out in Section IV. Correlations with CP-asymmetries in rare semileptonic decays are studied in Section V. We conclude in Section VI. Auxiliary information is given in several appendices.

II. CP-PHENOMENOLOGY IN CHARM

We review CP-violation in hadronic D -decays (Section II A), D -mixing (Section II B) and semileptonic $c \rightarrow u \ell^+ \ell^-$ processes (Section II C).

^{*}Electronic address: rigo.bause@tu-dortmund.de

[†]Electronic address: hector.gisbert@tu-dortmund.de

[‡]Electronic address: marcel.golz@tu-dortmund.de

[§]Electronic address: ghiller@physik.uni-dortmund.de

A. Direct CP-violation in $D^0 \rightarrow \pi^+ \pi^-, K^+ K^-$

The single-Cabibbo-suppressed (SCS) $D^0(\bar{D}^0)$ decay amplitudes $\mathcal{A}_f(\bar{\mathcal{A}}_f)$ to CP-eigenstates f can be written as

$$\begin{aligned}\mathcal{A}_f &= \mathcal{A}_f^T e^{i\phi_f^T} \left[1 + r_f e^{i(\delta_f + \phi_f)} \right], \\ \bar{\mathcal{A}}_f &= \eta_{\text{CP}} \mathcal{A}_f^T e^{-i\phi_f^T} \left[1 + r_f e^{i(\delta_f - \phi_f)} \right],\end{aligned}\quad (4)$$

where $\eta_{\text{CP}} = \pm 1$ is the CP-eigenvalue of f . The dominant SCS “tree” amplitude in the SM is denoted by $\mathcal{A}_f^T e^{\pm i\phi_f^T}$, and r_f parametrizes the relative magnitude of all subleading amplitudes. Inserting Eqs. (4) into Eq. (2), in the limit of $r_f \ll 1$, yields

$$A_{\text{CP}}(f) = -2r_f \sin \delta_f \sin \phi_f + \mathcal{O}(r_f^2), \quad (5)$$

requiring both strong (δ_f) and weak (ϕ_f) relative phases for a non-vanishing direct CP-asymmetry. Beyond the SM the SCS D^0 decay amplitude can be written as

$$\mathcal{A}_f = \sum_{q=d,s,b} \lambda_q (\mathcal{A}_f^q)_{\text{SM}} + \mathcal{A}_f^{\text{NP}}, \quad (6)$$

where the first term corresponds to the SM contribution with CKM-factors $\lambda_q = V_{cq}^* V_{uq}$ made explicit, and the second term accounts for NP. Using CKM unitarity $\lambda_d + \lambda_s + \lambda_b = 0$ and writing for the final states $K^+ K^-$ and $\pi^+ \pi^-$ in the subscripts $f = K$ and $f = \pi$, respectively, one finds

$$\begin{aligned}\mathcal{A}_{K(\pi)} &= \lambda_{s(d)} (\mathcal{A}_{K(\pi)}^{s(d)} - \mathcal{A}_{K(\pi)}^{d(s)})_{\text{SM}} \\ &\quad + \lambda_b (\mathcal{A}_{K(\pi)}^b - \mathcal{A}_{K(\pi)}^{d(s)})_{\text{SM}} + \mathcal{A}_{K(\pi)}^{\text{NP}}.\end{aligned}\quad (7)$$

Here, the first term is the SCS contribution and the second one corresponds to “penguin” contributions with small Wilson coefficients which are strongly CKM-suppressed with respect to the SCS one by $\lambda_b/\lambda_{s,d}$. The last term $\mathcal{A}_{K(\pi)}^{\text{NP}}$ encodes NP contributions. Using Eqs. (4), (5) and (7), we obtain

$$\Delta A_{\text{CP}} = \Delta A_{\text{CP}}^{\text{SM}} - \frac{2}{|\lambda_{s,d}|} \Delta r^{\text{NP}}, \quad (8)$$

where ¹

$$\Delta r^{\text{NP}} = r_K \sin \delta_K \sin \phi_K + r_\pi \sin \delta_\pi \sin \phi_\pi, \quad (9)$$

and

$$r_K = \frac{\mathcal{A}_K^{\text{NP}}}{(\mathcal{A}_K^d - \mathcal{A}_K^s)_{\text{SM}}}, \quad r_\pi = \frac{\mathcal{A}_\pi^{\text{NP}}}{(\mathcal{A}_\pi^d - \mathcal{A}_\pi^s)_{\text{SM}}}, \quad (10)$$

¹ The plus sign between the pion and kaon amplitudes in Eq. (9) comes from $\lambda_d = -\lambda_s + \mathcal{O}(\lambda_b)$.

and $r_{\pi,K} \ll 1$. The strong phases $\delta_{\pi,K}$ are associated with the NP amplitudes. Since we are interested in maximal NP contributions, we employ in our numerical analysis $\sin \delta_{\pi,K} \sim 1$. Note, there is a priori no information on the sign of Δr^{NP} as it depends on products of strong and weak phases. The branching ratios of the $D \rightarrow f$ modes are dominated by their respective SM contributions. We can therefore extract $|(\mathcal{A}_{K(\pi)}^{s(d)} - \mathcal{A}_{K(\pi)}^{d(s)})_{\text{SM}}|$ from data, see Appendix A for details.

B. CP-violation in $D^0 - \bar{D}^0$ mixing

Here we consider constraints from charm meson mixing. The $D^0 - \bar{D}^0$ transition amplitude can be written as

$$\langle D^0 | \mathcal{H}_{\text{eff}}^{\Delta c=2} | \bar{D}^0 \rangle = M_{12} - \frac{i}{2} \Gamma_{12}, \quad (11)$$

which can be parametrized in terms of the following physical quantities

$$x_{12} = 2 \frac{|M_{12}|}{\Gamma}, \quad y_{12} = \frac{|\Gamma_{12}|}{\Gamma}, \quad \phi_{12} = \arg \left(\frac{M_{12}}{\Gamma_{12}} \right). \quad (12)$$

Here, x_{12} and y_{12} are CP-conserving, while ϕ_{12} is a phase difference that results in CP-violation in mixing. A global fit from the HFLAV collaboration [2] results in

$$\begin{aligned}x_{12} &\in [0.22, 0.63] \%, \\ y_{12} &\in [0.50, 0.75] \%, \\ \phi_{12} &\in [-2.5^\circ, 1.8^\circ].\end{aligned}\quad (13)$$

In absence of a sufficiently controlled SM prediction of the mixing parameters, we require the NP contributions to saturate the current world averages (13),

$$x_{12}^{\text{NP}} \leq x_{12}, \quad x_{12}^{\text{NP}} \sin \phi_{12}^{\text{NP}} \leq x_{12} \sin \phi_{12}. \quad (14)$$

C. CP-violation in $c \rightarrow u \ell^+ \ell^-$

CP-violation in semileptonic rare charm decays arises from complex-valued Wilson coefficients $C_i^{\ell\ell}$, $C_i^{\ell\ell'}$ in the effective Hamiltonian [18],

$$\mathcal{H}_{\text{eff}} \supset -\frac{4G_F}{\sqrt{2}} \frac{\alpha_e}{4\pi} \sum_{i=9,10} (C_i^{\ell\ell} O_i^{\ell\ell} + C_i^{\ell\ell'} O_i^{\ell\ell'}) + \text{h.c.}, \quad (15)$$

with the operators

$$O_9^{\ell\ell(\prime)} = (\bar{u}_{L(R)} \gamma_\mu c_{L(R)}) (\bar{\ell} \gamma^\mu \ell), \quad (16)$$

$$O_{10}^{\ell\ell(\prime)} = (\bar{u}_{L(R)} \gamma_\mu c_{L(R)}) (\bar{\ell} \gamma^\mu \gamma_5 \ell). \quad (17)$$

Here, α_e denotes the fine structure constant, G_F is Fermi’s constant and $L = (1 - \gamma_5)/2$, $R = (1 + \gamma_5)/2$ are chiral projectors. CP-violation has not been observed

in semileptonic $|\Delta c| = |\Delta u| = 1$ decays yet. Available measurements for CP-asymmetries in rare semileptonic charm decays are at the level of few to $\mathcal{O}(10)\%$ [22], which is close to possible NP effects [13, 18, 21]. Branching ratio and high- p_T data imply the following constraints, barring cancellations [23, 24]

$$|C_{9,10}^{\mu\mu}{}^{(\prime)}| \lesssim 1, \quad |C_{9,10}^{ee}{}^{(\prime)}| \lesssim 3, \quad (18)$$

stronger for muons than for electrons.

III. A FLAVORFUL Z' IN CHARM

We work out NP-effects in charm from anomaly-free $U(1)'$ -extensions of the SM with fermion charges F_{ψ_i} that depend on the generation, $i = 1, 2, 3$. Specifically, SM fermion multiplets plus possibly right-handed neutrinos $\psi = Q, u, d, L, e, \nu$ in representations of $SU(3)_C \times SU(2)_L \times U(1)_Y \times U(1)'$ can be characterized, in that order, as

$$\begin{aligned} Q_i &= (3, 2, 1/6, F_{Q_i}), & u_i &= (3, 1, 2/3, F_{u_i}), \\ d_i &= (3, 1, -1/3, F_{d_i}), & L_i &= (1, 2, -1/2, F_{L_i}), \\ e_i &= (1, 1, -1, F_{e_i}), & \nu_i &= (1, 1, 0, F_{\nu_i}). \end{aligned} \quad (19)$$

Concrete models with F_{ψ_i} -assignments that fulfill the anomaly-cancellation conditions and induce $c \rightarrow u$ flavor changing neutral currents (FCNCs) are given in TABLE I. Related models (models 1 to 8) have been studied previously in the context of semileptonic rare charm decays in Ref. [18], to which we refer for further details. The models in TABLE I satisfy $\sum_{i=1}^3 (F_{Q_i} - F_{L_i} + 2F_{u_i} - F_{d_i} - F_{e_i}) = 0$ and therefore avoid kinetic mixing at one-loop [25].

In Section III A we discuss couplings of the fermions to the Z' -boson, which arises from the $U(1)'$ -group. We assume the Z' to have a mass $M_{Z'}$ of the electroweak scale or heavier. We discuss the induced $c \rightarrow u$ four-quark operators and Wilson coefficients in Section III B. In Section III C we discuss how to bypass constraints from $D^0 - \bar{D}^0$ mixing. We work out predictions for ΔA_{CP} in Section III D.

A. Z' -FCNCs

The Z' -couplings relevant to charm FCNCs can be written as

$$\begin{aligned} \mathcal{L}_{Z'} &\supset (g_L^{uc} \bar{u}_L \gamma^\mu c_L Z'_\mu + g_R^{uc} \bar{u}_R \gamma^\mu c_R Z'_\mu + \text{h.c.}) \\ &+ g_L^d \bar{d}_L \gamma^\mu d_L Z'_\mu + g_R^d \bar{d}_R \gamma^\mu d_R Z'_\mu \\ &+ g_L^s \bar{s}_L \gamma^\mu s_L Z'_\mu + g_R^s \bar{s}_R \gamma^\mu s_R Z'_\mu \\ &+ g_L^{\ell\ell} \bar{\ell}_L \gamma^\mu \ell_L Z'_\mu + g_R^{\ell\ell} \bar{\ell}_R \gamma^\mu \ell_R Z'_\mu, \end{aligned} \quad (20)$$

with $\ell = e, \mu, \tau$. The flavor diagonal couplings $g_{L,R}^{d,s}$ and $g_{L,R}^{\ell\ell}$ are given as the $U(1)'$ -gauge coupling g_4 times the associated charge F_ψ .

The $|\Delta c| = |\Delta u| = 1$ FCNC couplings $g_{L,R}^{uc}$ are generated via rotations from the gauge to the mass basis, and are in general complex-valued. Four different unitary rotations exist in the quark sector, corresponding to the left-handed (LH) and right-handed (RH) ones both for up- and down-type quarks. The product of LH up- and down-type rotations gives the CKM-matrix. In order to evade the severe constraints in the kaon sector, we assume the CKM-matrix to predominantly stem from the LH up-type rotation, implying

$$g_L^{uc} \approx g_4 \lambda_{\text{CKM}} \Delta F_L, \quad \Delta F_L = F_{Q_2} - F_{Q_1}, \quad (21)$$

where $\lambda_{\text{CKM}} \sim 0.2$ denotes the Wolfenstein parameter and we used $\lambda_{\text{CKM}} \ll 1$. In contrast, the RH rotation is a priori unconstrained and induces

$$g_R^{uc} = g_4 \sin \theta_u \cos \theta_u e^{i\phi_R} \Delta F_R, \quad (22)$$

where θ_u is the up-charm mixing angle for the up-quark singlets, $\Delta F_R = F_{u_2} - F_{u_1}$ and ϕ_R the corresponding CP-phase.

B. Four-fermion operators and matching

Generation-dependent quark-couplings result in additional operators in the effective weak Hamiltonian beyond the ones considered usually, *i.e.* Ref. [26]. At the scale $m_b < \mu < \mu_{\text{EWK}}$,

$$\mathcal{H}_{\text{eff}}^{|\Delta c|=1} \supset \frac{G_F}{\sqrt{2}} \sum_i \tilde{C}_i^{(\prime)} \tilde{Q}_i^{(\prime)} + \text{h.c.}, \quad (23)$$

with the new operators

$$\tilde{Q}_7 = (\bar{u}c)_{V-A} \sum_q F_{u_i, d_i} (\bar{q}q)_{V+A}, \quad (24)$$

$$\tilde{Q}_7' = (\bar{u}c)_{V+A} \sum_q F_{Q_i} (\bar{q}q)_{V-A}, \quad (25)$$

$$\tilde{Q}_8 = (\bar{u}_\alpha c_\beta)_{V-A} \sum_q F_{u_i, d_i} (\bar{q}_\beta q_\alpha)_{V+A}, \quad (26)$$

$$\tilde{Q}_8' = (\bar{u}_\alpha c_\beta)_{V+A} \sum_q F_{Q_i} (\bar{q}_\beta q_\alpha)_{V-A}, \quad (27)$$

$$\tilde{Q}_9 = (\bar{u}c)_{V-A} \sum_q F_{Q_i} (\bar{q}q)_{V-A}, \quad (28)$$

$$\tilde{Q}_9' = (\bar{u}c)_{V+A} \sum_q F_{u_i, d_i} (\bar{q}q)_{V+A}, \quad (29)$$

$$\tilde{Q}_{10} = (\bar{u}_\alpha c_\beta)_{V-A} \sum_q F_{Q_i} (\bar{q}_\beta q_\alpha)_{V-A}, \quad (30)$$

$$\tilde{Q}_{10}' = (\bar{u}_\alpha c_\beta)_{V+A} \sum_q F_{u_i, d_i} (\bar{q}_\beta q_\alpha)_{V+A}, \quad (31)$$

where $(V \pm A)$ refers to the Dirac structures $\gamma_\mu(1 \pm \gamma_5)$, $q = u, c, d, s, b$ and α, β are the color indices. The strength of these operators is given by their respective

model	F_{Q_i}			F_{u_i}			F_{d_i}			F_{L_i}			F_{e_i}			F_{ν_i}		
2	3	3	-6	-8	4	4	-10	10	0	-6	5	1	0	0	0	0	0	0
4	-1	-1	2	-1	2	-1	0	0	0	-1	1	0	-2	2	0	-2	-1	3
5	-1	-1	2	-1	2	-1	2	-1	-1	-1	1	0	-1	1	0	0	0	0
9	0	0	0	-11	-2	13	7	7	-14	-8	3	5	-6	16	-10	0	0	0
10	0	0	0	-13	6	7	-1	-14	15	-15	15	0	-14	18	-4	0	0	0
10 μ	0	0	0	-13	6	7	-1	-14	15	-15	0	15	-14	-4	18	0	0	0

TABLE I: Sample solutions of an anomaly-free $U(1)'$ -extension of the SM+3 ν_R with $F_{Q_1} = F_{Q_2}$. Models 2, 4 and 5 are taken from Ref. [18]. Models 9 and 10 feature $F_{Q_i} = 0$. In general, the ordering of generations is arbitrary due to permutation invariance. However, our analysis explicitly uses the ordering stated here, that is, the i th entry corresponds to the i th generation. Model 10 μ is the same as model 10 with the smallest lepton-coupling to muons.

Wilson coefficients \tilde{C}_i , \tilde{C}'_i which depend on both heavy masses and weak phases responsible for CP-violating phenomena. The Wilson coefficients induced by the Lagrangian (20) read

$$\begin{aligned}\tilde{C}_7(M_{Z'}) &= \tilde{C}_9(M_{Z'}) = \frac{\sqrt{2}}{G_F} g_L^{uc} \frac{g_4}{4 M_{Z'}^2}, \\ \tilde{C}'_7(M_{Z'}) &= \tilde{C}'_9(M_{Z'}) = \frac{\sqrt{2}}{G_F} g_R^{uc} \frac{g_4}{4 M_{Z'}^2}, \\ \tilde{C}_8^{(\prime)}(M_{Z'}) &= \tilde{C}_{10}^{(\prime)}(M_{Z'}) = 0.\end{aligned}\quad (32)$$

They are evolved from $M_{Z'}$ to m_c using the renormalization group equations (RGEs) with top and bottom quarks integrated out at their respective threshold scales. Finite values of $\tilde{C}_8^{(\prime)}$ and $\tilde{C}_{10}^{(\prime)}$ arise from the RGE mixing at the charm mass scale, see Appendix B for details.

C. $D^0 - \bar{D}^0$ mixing constraints

Rare $|\Delta c| = |\Delta u| = 1$ decays are induced in the Z' -models by operators with coefficients proportional to g_L^{uc} or g_R^{uc} in Eq. (32). These couplings induce at second order $D^0 - \bar{D}^0$ mixing (13), and are constrained as

$$|(g_L^{uc})^2 + (g_R^{uc})^2 - X g_L^{uc} g_R^{uc}| \lesssim 6 \cdot 10^{-7} \left(\frac{M_{Z'}}{\text{TeV}} \right)^2, \quad (33)$$

with $X \sim 20$ for $M_{Z'}$ in the TeV range [18]. This constraint on x_{12} can be evaded if both g_L^{uc} and g_R^{uc} are present, for either $g_L^{uc} \sim X g_R^{uc}$ or $g_L^{uc} \sim 1/X g_R^{uc}$. However, in these cases the CP-phases have to be aligned $\text{Arg}(g_L^{uc}) \sim \text{Arg}(g_R^{uc})$ to fulfill Eq. (33). As kaon constraints force $\text{Arg}(g_L^{uc})$ to be SM-like, CP-violating effects in charm become negligible.

We therefore choose $g_L^{uc} = 0$, which can be achieved with $\Delta F_L = 0$. The models in TABLE I satisfy for this reason $F_{Q_1} = F_{Q_2}$. Consequently, we focus on FCNCs in the up-singlet sector (22), that is, $g_R^{uc} \neq 0$ and complex. If there is a single coupling only, the above mixing con-

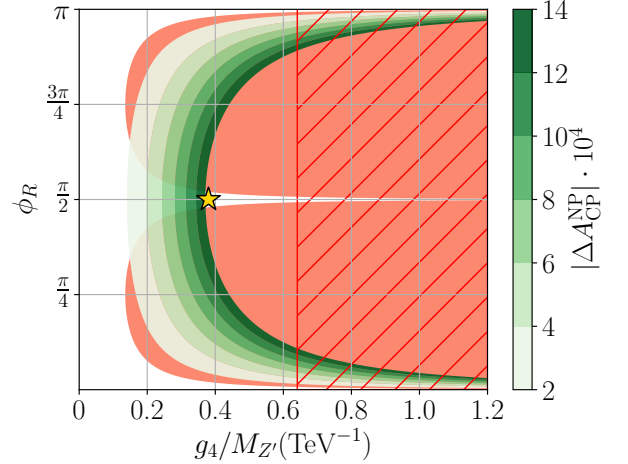


FIG. 1: $|\Delta A_{\text{CP}}^{\text{NP}}|$ (green bands) versus $D^0 - \bar{D}^0$ mixing exclusion regions (14) on the imaginary part $x_{12} \sin \phi_{12}$ (red area) and the absolute value x_{12} (red hatched area) in the $\phi_R - g_4/M_{Z'}$ (TeV^{-1}) plane for $\theta_u = 1 \cdot 10^{-4}$. F_ψ -charges are as in model 2, see TABLE I. The golden star indicates a benchmark point (40), see text for details.

straint on x_{12} becomes

$$|g_A^{uc}| \lesssim 8 \cdot 10^{-4} \left(\frac{M_{Z'}}{\text{TeV}} \right), \quad A = L, R. \quad (34)$$

The even tighter constraint (14) for CP-violating couplings on $x_{12} \sin \phi_{12}$ can be bypassed for $\text{Arg}(g_R^{uc}) = \phi_R$ around $\pi/2$ (or $3\pi/2$), as the CP-phase of the mixing amplitude is twice the one of the $|\Delta c| = |\Delta u| = 1$ FCNC [26]. The contributions to ΔA_{CP} become maximal while simultaneously mixing constraints are satisfied. This interplay of ϕ_R versus the coupling $g_4/M_{Z'}$ (TeV^{-1}) for model 2 and fixed $\theta_u = 1 \cdot 10^{-4}$ is illustrated in FIG. 1. The red (hatched) area corresponds to the $D^0 - \bar{D}^0$ mixing constraints on the imaginary part $x_{12} \sin \phi_{12}$ (absolute value x_{12}). Z' -induced values of ΔA_{CP} are shown in green. Indeed the region around $\phi_R \sim \pi/2$ is viable and can induce $\Delta A_{\text{CP}}^{\text{NP}} \sim 10^{-3}$.

D. Z' -effects for ΔA_{CP}

Taking into account the running from $M_{Z'}$ to m_c , details of which are given in Appendix B, we find that ΔA_{CP} can be written as

$$\Delta A_{\text{CP}}^{\text{NP}} = A_{\text{CP}}^{\text{NP}}(K^+ K^-) - A_{\text{CP}}^{\text{NP}}(\pi^+ \pi^-), \quad (35)$$

with

$$\begin{aligned} A_{\text{CP}}^{\text{NP}}(K^+ K^-) &\sim \frac{g_4^2}{M_{Z'}^2} \theta_u \Delta F_R [c_K F_{Q_2} + d_K F_{d_2}], \\ A_{\text{CP}}^{\text{NP}}(\pi^+ \pi^-) &\sim \frac{g_4^2}{M_{Z'}^2} \theta_u \Delta F_R [c_\pi F_{Q_1} + d_\pi F_{d_1}], \end{aligned} \quad (36)$$

where

$$\begin{aligned} c_K &= \frac{\chi_K}{a_K} r_1(m_c, M_{Z'}) , \quad c_\pi = -\frac{\chi_\pi}{a_\pi} r_1(m_c, M_{Z'}) , \\ d_K &= \frac{1}{a_K} r_2(m_c, M_{Z'}) , \quad d_\pi = -\frac{1}{a_\pi} r_2(m_c, M_{Z'}) . \end{aligned} \quad (37)$$

As explained in the previous Section III C, we analyze models with $g_L^{uc} = 0$ and $\text{Im}(g_R^{uc})$ large. In Eq. (36) we use $\sin \delta_{\pi, K} \sin \phi_R \sim 1$ and anticipated $\theta_u \ll 1$. The parameters $c_{K, \pi}$ and $d_{K, \pi}$ depend on the chiral factors $\chi_{K, \pi}$ at the charm scale, the LO QCD running functions $r_{1,2}(m_c, M_{Z'})$ and the tree-level contributions $a_{K, \pi}$, which are determined experimentally. Further details can be found in Appendices A–D. Numerical values of $c_{K, \pi}$ and $d_{K, \pi}$ for different Z' masses are displayed in TABLE II.

$M_{Z'} [\text{TeV}]$	2	4	6	8	10
c_K	1.133	1.217	1.266	1.302	1.330
d_K	-0.046	-0.054	-0.058	-0.061	-0.063
c_π	-1.446	-1.553	-1.616	-1.661	-1.698
d_π	0.058	0.068	0.074	0.077	0.080
$d_{\pi'}$	0.071	0.083	0.090	0.094	0.098
d_{π^0}	0.077	0.090	0.097	0.102	0.106

TABLE II: Parameters $c_{K, \pi}$, $d_{K, \pi}$ and d_{π', π^0} in $(\text{TeV})^2$ as defined in Eq. (37) and Eq. (53), respectively, for different Z' masses.

In FIG. 2 we show sizable Z' -contributions to $\Delta A_{\text{CP}}^{\text{NP}}$ and $D^0 - \bar{D}^0$ mixing constraints (red area) in the plane of $g_4/M_{Z'} (\text{TeV}^{-1})$ and the parameter $\Delta \tilde{F}_R = \Delta F_R \theta_u$ for models 2, 5, 9 and $10(\mu)$. The corresponding plot of model 4 is not given in FIG. 2 because it exhibits very similar bands as model 5 due to identical $F_{Q_{1,2}}$ and ΔF_R , as shown in TABLE I. Constraints from branching ratios of (semi-)muonic D -decays (dash-dotted and

dotted lines), here for $g_L^{uc} = 0$, [18]

$$\begin{aligned} &|g_R^{uc}| \sqrt{(g_L^{\mu\mu})^2 + (g_R^{\mu\mu})^2} \\ &= g_4^2 |\Delta \tilde{F}_R| \sqrt{F_{L_2}^2 + F_{e_2}^2} \lesssim 0.04 \left(\frac{M_{Z'}}{\text{TeV}} \right)^2, \end{aligned} \quad (38)$$

$$\begin{aligned} &|g_R^{uc}(g_L^{\mu\mu} - g_R^{\mu\mu})| \\ &= g_4^2 |\Delta \tilde{F}_R (F_{L_2} - F_{e_2})| \lesssim 0.03 \left(\frac{M_{Z'}}{\text{TeV}} \right)^2, \end{aligned} \quad (39)$$

start to be competitive with mixing constraints close to the non-perturbativity region (black region). This is particularly relevant for model 9 and 10, which exhibit large couplings to leptons. To evade the muon constraints and allow for slightly larger values of ΔA_{CP} we also consider model 10μ , which is the same as model 10 with the lepton-charges ordered in such a way that the smallest ones are for muons, stressing the interplay between hadronic and leptonic sectors; model 10 can accommodate $\Delta A_{\text{CP}}^{\text{NP}}$ up to $1.5 \cdot 10^{-3}$, while model 10μ can reach $1.8 \cdot 10^{-3}$. FIG. 2 shows the stronger bound for each model, *i.e.*, Eq. (39) for models 2, 5, 9 and 10μ (dash-dotted) and Eq. (38) for model 10 (dotted).

In FIGS. 1 and 2 we show benchmark points. They pass constraints from D -mixing and semi(-muonic) decays, while giving $\Delta A_{\text{CP}}^{\text{NP}} \sim 10^{-3}$. The golden star corresponds to model 2 with $\Delta F_R = 12$ and

$$\phi_R \sim \pi/2, \quad g_4/M_{Z'} \sim 0.38/\text{TeV}, \quad \theta_u \sim 1 \cdot 10^{-4}. \quad (40)$$

The pink diamond corresponds to model 10μ with $\Delta F_R = 19$ and

$$\phi_R \sim \pi/2, \quad g_4/M_{Z'} \sim 2.3/\text{TeV}, \quad \theta_u \sim 1.7 \cdot 10^{-5}. \quad (41)$$

We learn that Z' -models with charges as in TABLE I can provide concrete NP-interpretations of ΔA_{CP} of the order of 10^{-3} . $D^0 - \bar{D}^0$ mixing provides upper limits on the achievable $\Delta A_{\text{CP}}^{\text{NP}}$. To distinguish the different model scenarios we explore correlations of ΔA_{CP} with other sectors, hadronic 2-body D -decays in Section IV and semileptonic $c \rightarrow u \ell^+ \ell^-$ transitions in Section V.

IV. PATTERNS IN HADRONIC DECAYS

Z' -models with non-universal charges F_ψ can give rise to large flavor-breaking effects which could explicitly violate relations between hadronic charm decays [28–31]. We study signatures of Z' -induced U-spin and isospin breaking in Section IV A and Section IV B, respectively. A_{CP} in $D^0 \rightarrow \pi^0 \pi^0$ is studied in Section IV C.

A. U-spin patterns in $D^0 \rightarrow \pi^+ \pi^-, K^+ K^-$

U-spin breaking arises for $F_{Q_1} \neq F_{Q_2}$ or $F_{d_1} \neq F_{d_2}$, and can upset the U-spin sum rule [28]

$$A_{\text{CP}}(D^0 \rightarrow K^+ K^-) + A_{\text{CP}}(D^0 \rightarrow \pi^+ \pi^-) = 0. \quad (42)$$

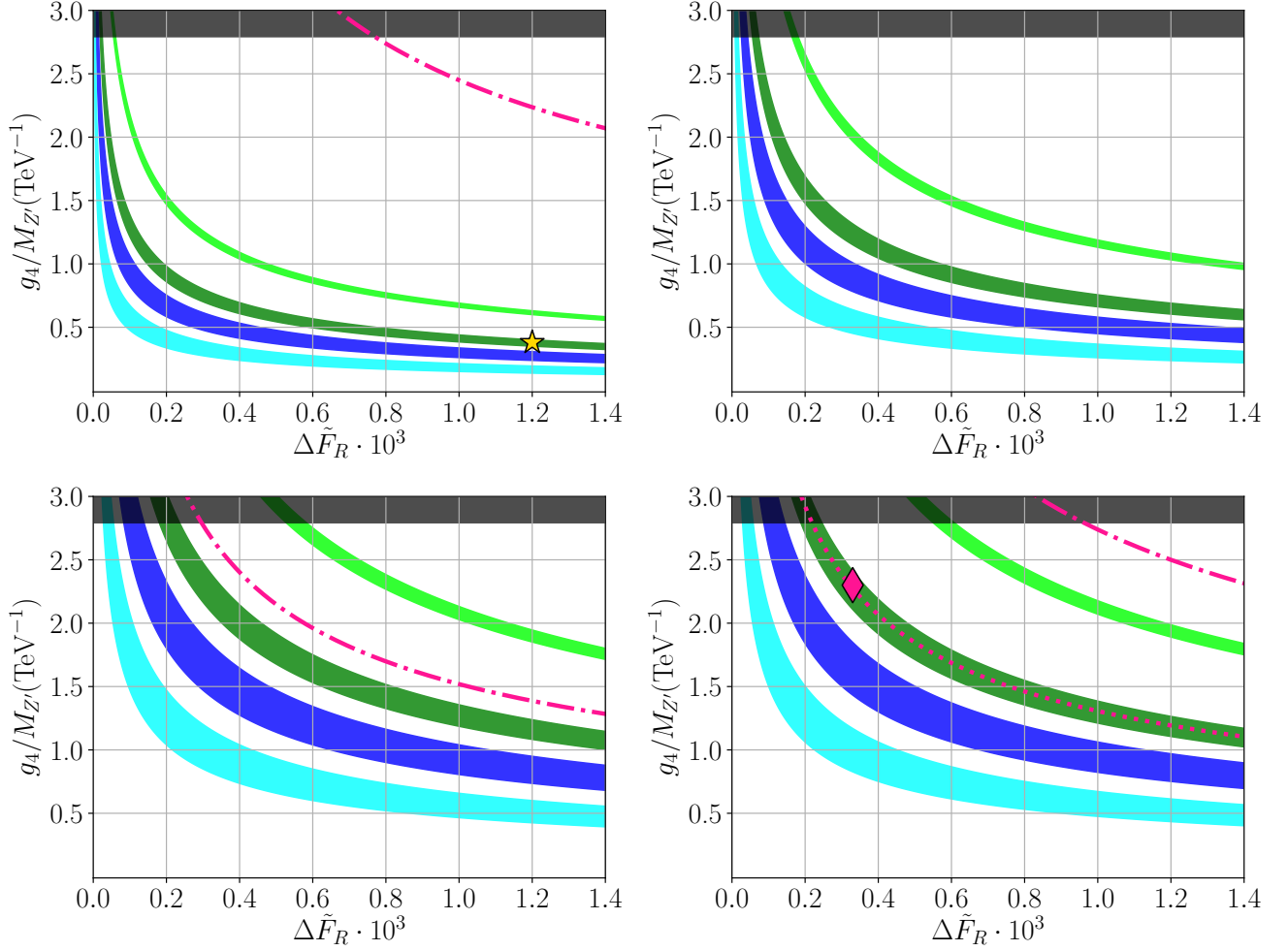


FIG. 2: $|\Delta A_{\text{CP}}^{\text{NP}}|$ for different Z' -models (2 upper left, 5 upper right, 9 lower left and $10(\mu)$ lower right) in the plane of $g_4/M_{Z'} (\text{TeV}^{-1})$ and $\Delta \tilde{F}_R = \Delta F_R \cdot \theta_u$, together with the excluded region from $D^0-\bar{D}^0$ mixing (red). Light green, dark green, blue and cyan bands correspond to $|\Delta A_{\text{CP}}^{\text{NP}}| = (4.0 \pm 0.2) \cdot 10^{-3}$, $|\Delta A_{\text{CP}}^{\text{NP}}| = (1.5 \pm 0.2) \cdot 10^{-3}$, $|\Delta A_{\text{CP}}^{\text{NP}}| = (8 \pm 2) \cdot 10^{-4}$ and $|\Delta A_{\text{CP}}^{\text{NP}}| = (3 \pm 1) \cdot 10^{-4}$, respectively. The black region indicates the upper bound coming from perturbativity and direct searches in dimuon and dielectron spectra [27], which read $g_4 \leq 4\pi$ and $M_{Z'} \geq 4.5 \text{ TeV}$, respectively. The magenta dash-dotted and dotted lines show the stronger (if any) of the bounds from Eqs. (38) and (39). In the lower right plot the dotted line corresponds to model 10, and the dash-dotted to model 10μ . The golden star and pink diamond are benchmark points (40) and (41). See text for details.

To quantify deviations from this relation we define ²

$$U_{\text{break}}^{\text{tot}} = \left| 1 + \frac{A_{\text{CP}}(D^0 \rightarrow K^+ K^-)}{A_{\text{CP}}(D^0 \rightarrow \pi^+ \pi^-)} \right|. \quad (43)$$

In the U-spin limit $U_{\text{break}}^{\text{tot}} = 0$.

² For model $10(\mu)$ we use instead $\left| 1 + \frac{A_{\text{CP}}(D^0 \rightarrow \pi^+ \pi^-)}{A_{\text{CP}}(D^0 \rightarrow K^+ K^-)} \right|$ to avoid $U_{\text{break}}^{\text{tot}} > 1$. It is tacitly understood that K, Q_2, d_2 and π, Q_1, d_1 -indices in Eq. (44) and following need to be swapped in this case.

Using Eqs. (36), $U_{\text{break}}^{\text{tot}}$ can be written as

$$U_{\text{break}}^{\text{tot}} = \left| 1 + \frac{c_K F_{Q_2} + d_K F_{d_2}}{c_\pi F_{Q_1} + d_\pi F_{d_1}} \right|. \quad (44)$$

In TABLE III we give $U_{\text{break}}^{\text{tot}}$ for models 2, 4, 5, 9 and $10(\mu)$, for $M_{Z'} = 6 \text{ TeV}$. The variation of $U_{\text{break}}^{\text{tot}}$ with $M_{Z'}$ in the range shown is within a few percent.

Taking advantage of the smallness of the parameters $d_{K,\pi}$ relative to $c_{K,\pi}$, we perform a Taylor expansion in Eq. (44) up to $\mathcal{O}(d_K, d_\pi)$ to qualitatively understand how U-spin breaking in our models emerges. This leads to

$$U_{\text{break}}^{\text{tot}} \approx \left| 1 + \frac{c_K}{c_\pi} - \frac{c_K d_\pi F_{d_1}}{c_\pi^2 F_{Q_1}} + \frac{d_K F_{d_2}}{c_\pi F_{Q_1}} \right|, \quad (45)$$

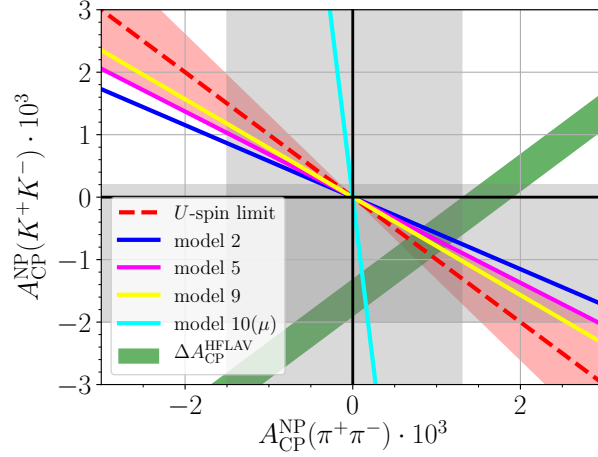


FIG. 3: $A_{\text{CP}}(K^+K^-)$ versus $A_{\text{CP}}(\pi^+\pi^-)$ with predictions in the Z' -models 2, 5, 9 and $10(\mu)$ in blue, magenta, yellow and cyan lines, respectively. The green band corresponds to the experimental world average of ΔA_{CP} (3) at 1σ . The gray bands indicate the present experimental 1σ regions given in TABLE IV. The U-spin limit (42) (red dashed line) and $\lesssim 30\%$ SM-like U-spin breaking (red area) is also shown.

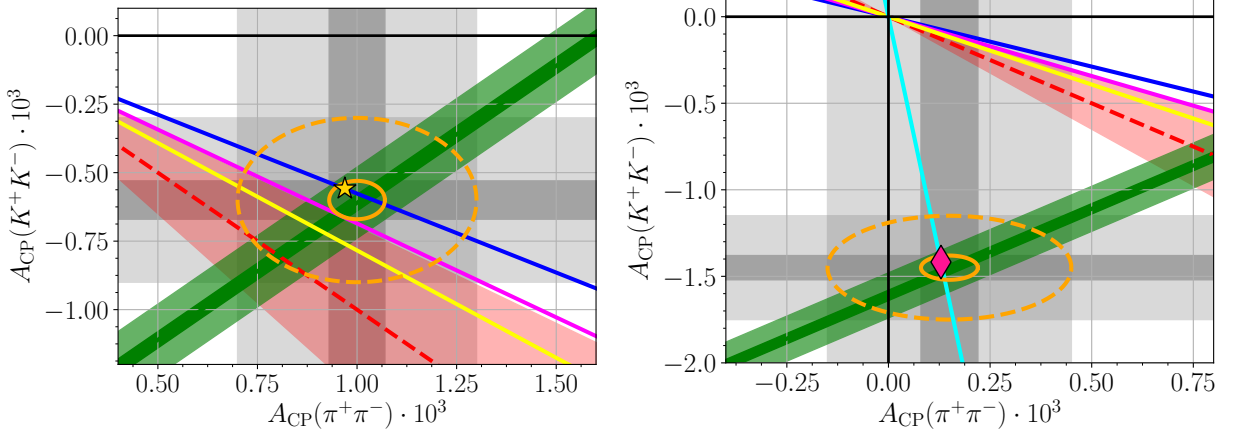


FIG. 4: Future projections for $A_{\text{CP}}(K^+K^-)$ versus $A_{\text{CP}}(\pi^+\pi^-)$ with predictions in the Z' -models 2, 5, 9 and $10(\mu)$ in blue, magenta, yellow and cyan lines, respectively. The green band corresponds to the central value of the present experimental world average of ΔA_{CP} (3) with future 1σ sensitivities according to TABLE IV. The gray bands illustrate two future measurements of the individual asymmetries. The central values are given in Eq. (50), the uncertainties are scaled according to TABLE IV. Lighter (darker) bands correspond to LHCb Run 1-3 (1-5). Assuming for simplicity gaussian errors a dashed (solid) ellipse occurs around model 2 (plot to the left) and model 10μ (plot to the right) for LHCb Run 1-3 (1-5). The U-spin limit (42) (red dashed line) and $\lesssim 30\%$ SM-like U-spin breaking (red area) is also shown. The golden star and pink diamond are benchmark points (40) and (41).

for $F_{Q_1} = F_{Q_2} \neq 0$ (models 2, 4 and 5), while for $F_{Q_1} = F_{Q_2} = 0$ (models 9 and $10(\mu)$) Eq. (44) simply becomes

$$U_{\text{break}}^{\text{tot}} = \left| 1 + \frac{d_K F_{d_2}}{d_\pi F_{d_1}} \right|. \quad (46)$$

For models with $F_{Q_1} = F_{Q_2} \neq 0$ different sources of U-spin breaking exist. The second term in Eq. (45) accounts for effects originating from interference between the SM-amplitude and the $F_{Q_{1,2}}$ -charges. This contribution is responsible for 22% U-spin breaking, which is of the same order of magnitude as the expected U-

spin breaking uncertainty of the SM. In contrast, the last two terms in Eq. (45) are pure NP U-spin breaking effects. Eq. (45) can further be simplified with $d_K \approx \frac{c_K}{c_\pi} d_\pi$ due to $\chi_\pi \approx \chi_K$, which holds numerically at the level of $\mathcal{O}(0.1 - 1)\%$. It follows that

$$U_{\text{break}}^{\text{tot}} \approx \left| 1 + \frac{c_K}{c_\pi} + \frac{d_K}{c_\pi} \left(\frac{F_{d_2} - F_{d_1}}{F_{Q_1}} \right) \right|, \quad (47)$$

highlighting that pure NP U-spin breaking effects are

model	$\beta_9^{\mu\mu}$	$\beta_{10}^{\mu\mu}$	β_9^{ee}	β_{10}^{ee}	β_{π^0}	$\beta_{\pi'}$	$U_{\text{break}}^{\text{tot}}$
2	0.57	-0.57	-0.68	0.68	-0.02	-0.02	0.42
4	-1.04	-0.35	1.04	0.35	-0.03	-0.03	0.22
5	-0.67	0	0.67	0	-0.10	-0.09	0.32
9	-20.56	-14.07	15.15	-2.17	-1.89	-1.75	0.22
10	37.25	3.39	-32.73	1.13	1.31	1.22	0.91
10μ	-4.52	-4.52	-32.73	1.13	1.31	1.22	0.91

TABLE III: Values of $\beta_{9/10}^{\ell\ell}$ in $(\text{TeV})^{-2}$ for $\ell = \mu, e$ and dimensionless $\beta_{\pi',0}$ as defined in Eq. (63) and Eq. (55), respectively, as well as $U_{\text{break}}^{\text{tot}}$ in Eq. (44), see footnote 2, for $M_{Z'} = 6 \text{ TeV}$.

$\times 10^{-4}$	Data	σ_{LHCb}	$\sigma_{\text{Belle II}}$
ΔA_{CP}	-15.4 ± 2.9 [1]	1.3 (0.3)	–
$\Delta A_{\text{CP}}^{\text{HFLAV}}$	-16.4 ± 2.8 [2]	1.3 (0.3)	–
$A_{\text{CP}}(D^0 \rightarrow K^+ K^-)$	-9 ± 11 [2]	3 (0.7)	3
$A_{\text{CP}}(D^0 \rightarrow \pi^+ \pi^-)$	-1 ± 14 [2]	3 (0.7)	5
$A_{\text{CP}}(D^0 \rightarrow \pi^0 \pi^0)$	-3 ± 64 [2]	–	9
$A_{\text{CP}}(D^+ \rightarrow \pi^+ \pi^0)$	$+290 \pm 290 \pm 30$ [32]	–	17

TABLE IV: CP-asymmetries and future sensitivities σ in units of 10^{-4} at LHCb Run 1-3 (Run 1-5) [33] and Belle II with 50 ab^{-1} [34].

induced by

$$U_{\text{break}}^{\text{NP}} = \frac{d_K}{c_\pi} \left| \frac{F_{d_2} - F_{d_1}}{F_{Q_1}} \right| \approx 0.04 \left| \frac{F_{d_2} - F_{d_1}}{F_{Q_1}} \right|, \quad (48)$$

which indicates how both the pion chiral enhancement and r_2 suppress U-spin breaking in these models. Therefore, values of $F_{d_2} - F_{d_1} \sim \mathcal{O}(1)$ such as in model 5, induce U-spin breaking within the range expected within the SM $\lesssim 30\%$. In model 4, $F_{d_i} = 0$ and $U_{\text{break}}^{\text{NP}} = 0$, that is, U-spin breaking is SM-like. On the other hand, for $F_{d_2} - F_{d_1} \sim \mathcal{O}(10)$ as in model 2, large U-spin breaking effects can arise and would be discernible with future sensitivities for $A_{\text{CP}}(K^+ K^-)$ and $A_{\text{CP}}(\pi^+ \pi^-)$ shown in TABLE IV.

For models with $F_{Q_1} = F_{Q_2} = 0$ we obtain for the pure NP U-spin breaking from Eq. (46)

$$U_{\text{break}}^{\text{NP}}(F_{Q_{1,2}} = 0) \approx 0.78 \left| \frac{F_{d_2} - F_{d_1}}{F_{d_1}} \right|, \quad (49)$$

which, unlike in Eq. (48), is unsuppressed. Models with $F_{Q_1} = F_{Q_2} = 0$ are therefore prime candidates for sizable NP U-spin breaking effects. Models 9 and $10(\mu)$ have been constructed for this purpose. However, in model 9 $F_{d_2} = F_{d_1}$ and U-spin breaking arises from $d_K \neq -d_\pi$ only, and is SM-like.

Note, the strong phases associated with NP are assumed to be similar, $\sin \delta_\pi \simeq \sin \delta_K$, and order one; violation of Eq. (42) can be suppressed or even further enhanced by U-spin breaking in the strong phases. While this is an uncertainty on the NP interpretation, Z' -signals could even be more striking.

In FIGs. 3 and 4 we show the contributions of models 2, 5, 9 and $10(\mu)$ to the individual CP-asymmetries $A_{\text{CP}}(K^+ K^-)$ and $A_{\text{CP}}(\pi^+ \pi^-)$ in blue, magenta, yellow and cyan, respectively. The U-spin limit is given by the red dashed line with 30% U-spin breaking indicated by the red contour. Present experimental bounds from TABLE IV are shown in FIG. 3 as 1σ regions in gray for the individual asymmetries and in green for ΔA_{CP} . The future sensitivities are indicated in light (dark) gray and green bands in FIG. 4 for LHCb Run 1-3 (1-5). We use the following central values for the plot to the left (right)

$$\begin{aligned} A_{\text{CP}}^{\text{cen}}(K^+ K^-) &= -0.6 \cdot 10^{-3} \left(-1.45 \cdot 10^{-3} \right), \\ A_{\text{CP}}^{\text{cen}}(\pi^+ \pi^-) &= 1.0 \cdot 10^{-3} \left(0.15 \cdot 10^{-3} \right). \end{aligned} \quad (50)$$

The orange error ellipses illustrate the NP sensitivity of the projected uncertainties of $A_{\text{CP}}(K^+ K^-)$ and $A_{\text{CP}}(\pi^+ \pi^-)$ assuming no correlations. A future data-based analysis which takes into account correlations between the individual asymmetries and ΔA_{CP} can be expected to be more powerful.

U-spin symmetry within the SM is broken at the level of 30%. We find that flavorful Z' -models can exceed this by far (model $10(\mu)$), or moderately (model 2), which makes the measurements of $A_{\text{CP}}(K^+ K^-)$ and $A_{\text{CP}}(\pi^+ \pi^-)$ smoking guns for NP, within reach of Belle II and LHCb with the projected sensitivities.

B. Isospin breaking patterns in $D^+ \rightarrow \pi^+ \pi^0$

Isospin breaking arises in Z' -models if $F_{u_1} \neq F_{d_1}$. In charm physics, the hadronic decay $D^+ \rightarrow \pi^+ \pi^0$ represents a formidable candidate to study these effects, because the CP-asymmetry $A_{\text{CP}}(\pi^+ \pi^0)$, defined by

$$A_{\text{CP}}(\pi^+ \pi^0) = \frac{\Gamma(D^+ \rightarrow f^+) - \Gamma(D^- \rightarrow f^-)}{\Gamma(D^+ \rightarrow f^+) + \Gamma(D^- \rightarrow f^-)}, \quad (51)$$

with $f^\pm = \pi^\pm \pi^0$ is a clean SM null test [35].

Following the same procedure as in Section IIID for $\Delta A_{\text{CP}}^{\text{NP}}$ we obtain, using $\theta_u \ll 1$,

$$A_{\text{CP}}^{\text{NP}}(\pi^+ \pi^0) \sim \frac{g_4^2}{M_{Z'}^2} \theta_u \Delta F_R d_{\pi'} (F_{d_1} - F_{u_1}), \quad (52)$$

with

$$d_{\pi'} = -\frac{1}{a_{\pi'}} r_2(m_c, M_{Z'}) . \quad (53)$$

Here, $a_{\pi'}$ denotes the tree-level contribution to $D^+ \rightarrow \pi^+ \pi^0$ whose modulus has been fixed experimentally, see Appendix A for details. Numerical values of $d_{\pi'}$ for different values of $M_{Z'}$ are given in TABLE II. Inserting Eq. (35) into Eq. (52), we obtain

$$A_{\text{CP}}^{\text{NP}}(\pi^+ \pi^0) \sim \beta_{\pi'} \cdot \Delta A_{\text{CP}}^{\text{NP}}, \quad (54)$$

where

$$\beta_{\pi'} = \frac{d_{\pi'}(F_{d_1} - F_{u_1})}{c_K F_{Q_2} + d_K F_{d_2} - c_\pi F_{Q_1} - d_\pi F_{d_1}}. \quad (55)$$

Values of $\beta_{\pi'}$ for $M_{Z'} = 6$ TeV and different Z' -models can be seen in TABLE III. Since we have lost information about the signs of the leading SM decay amplitudes with which NP is interfering, we cannot predict the relative sign between the CP-asymmetries in Eq. (54) without relying on assumptions on the strong interaction. Note, unlike for $A_{\text{CP}}(K^+ K^-)$ and $A_{\text{CP}}(\pi^+ \pi^-)$, there is no SM flavor symmetry here at work.

We find that model 9 and 10(μ) induce values near

$$A_{\text{CP}}^{\text{NP}}(\pi^+ \pi^0) \sim (1 - 2) \cdot \Delta A_{\text{CP}}^{\text{NP}}, \quad (56)$$

which for $\Delta A_{\text{CP}}^{\text{NP}} \sim 10^{-3}$ is within the projected sensitivity of Belle II with 50 ab^{-1} [34], see TABLE IV. Model 2, 4 and 5 induce $A_{\text{CP}}^{\text{NP}}(\pi^+ \pi^0) \lesssim 0.1 \cdot \Delta A_{\text{CP}}^{\text{NP}} \sim 10^{-4}$, beyond the reach of current facilities.

This behavior can be understood by expanding Eq. (55) in the d_i up to $\mathcal{O}(d_i)$. For $F_{Q_1} = F_{Q_2} = 0$ (model 9 and 10(μ)), we find that $\beta_{\pi'}$ scales with $d_{\pi'}/d_K \approx -1.6$ times a combination of charges $(F_{d_1} - F_{u_1})/F_{d_2}(1 + \dots) \sim \mathcal{O}(1)$ resulting in $\mathcal{O}(1)$ isospin breaking effects. For models with $F_{Q_1} = F_{Q_2} \neq 0$ instead a suppression factor $d_{\pi'}/(c_K - c_\pi) \approx 0.03$ exists from the chiral enhancement of the $(V - A) \times (V + A)$ operators, leading to $\beta_{\pi'}$ of $\mathcal{O}(10^{-2} - 10^{-1})$.

C. $D^0 \rightarrow \pi^0 \pi^0$

We work out the CP-asymmetry for $D^0 \rightarrow \pi^0 \pi^0$ decays because of its potential to diagnose patterns of NP [36]. In addition, the experimental prospect at Belle II for $A_{\text{CP}}(D^0 \rightarrow \pi^0 \pi^0)$ is about a factor of two better than for $A_{\text{CP}}(D^+ \rightarrow \pi^+ \pi^0)$, see TABLE IV. In the Z' -models, $A_{\text{CP}}(D^0 \rightarrow \pi^0 \pi^0)$ is obtained from Eqs. (52) and (53) after replacing subscripts π' by π^0 with otherwise identical expressions. Therefore, with β_{π^0} given in TABLE III,

$$A_{\text{CP}}^{\text{NP}}(\pi^0 \pi^0) \sim \beta_{\pi^0} \cdot \Delta A_{\text{CP}}^{\text{NP}}, \quad (57)$$

hence

$$A_{\text{CP}}^{\text{NP}}(\pi^0 \pi^0) \lesssim 2 \cdot \Delta A_{\text{CP}}^{\text{NP}}, \quad (58)$$

with the limit saturated by model 9, and which is within the sensitivity of Belle II with 50 ab^{-1} [34], see TABLE IV. Furthermore,

$$\frac{A_{\text{CP}}^{\text{NP}}(\pi^0 \pi^0)}{A_{\text{CP}}^{\text{NP}}(\pi^+ \pi^0)} \sim \frac{\beta_{\pi^0}}{\beta_{\pi'}} = \frac{a_{\pi'}}{a_{\pi^0}} = 1.08 \pm 0.10, \quad (59)$$

holds universally for all Z' -models with $F_{u_1} \neq F_{d_1}$. Experimental tests of Eq. (59) can support a Z' -interpretation, however, additional uncertainties from large, unknown strong phases exist, which can modify the relation. As discussed after Eq. (54), we cannot predict the relative sign between the CP-asymmetries (57), (59) without relying on input on the strong interaction.

V. SEMILEPTONIC DECAYS VS. ΔA_{CP}

The dominant Wilson coefficients in $c \rightarrow u \ell^+ \ell^-$ transitions are $C_{9/10}^{\ell\ell'}$, defined in Eq. (15). In flavorful Z' -models [18]

$$C_{9/10}^{\ell\ell'}(M_{Z'}) = -\frac{\pi}{\sqrt{2} G_F \alpha_e} \frac{g_L^{uc}}{M_{Z'}^2} (g_R^{\ell\ell} \pm g_L^{\ell\ell}), \quad (60)$$

$$C_{9/10}^{\ell\ell'}(M_{Z'}) = -\frac{\pi}{\sqrt{2} G_F \alpha_e} \frac{g_R^{uc}}{M_{Z'}^2} (g_R^{\ell\ell} \pm g_L^{\ell\ell}), \quad (61)$$

where $g_R^{\ell\ell} = g_4 F_{e_i}$ and $g_L^{\ell\ell} = g_4 F_{L_i}$ with in general different couplings for muons and electrons. As explained in Section III C, we analyze in this work Z' -models with $g_L^{uc} = 0$ and $\text{Im}(g_R^{uc})$ large.

CP-asymmetries in the branching ratios are induced by interference of NP, here through g_R^{uc} , with C_9^{eff} , the effective coefficient of O_9 present in the SM, which is lepton-universal, depends on the dilepton invariant mass and has sizable hadronic contributions and provides sizable strong phases. This interference term is sensitive to $C_9^{\ell\ell'}$ only. Angular analysis offers further opportunities. An interesting recent example for the latter is $D^0 \rightarrow \pi^+ \pi^- \mu^+ \mu^-$ decays [21, 22, 37]. Notably, the angular observables $I_{5,6,7}$ are GIM-protected in the SM and clean null tests [21]. In the Z' -models under consideration, $I_{5,6}$ are induced by $\text{Re}(C_9^{\ell\ell'} \cdot C_{10}^{\ell\ell'*})$ and $\text{Im}(C_{10}^{\ell\ell'} \cdot C_9^{\text{eff}*})$, whereas I_7 is induced by $\text{Re}[(C_9^{\text{eff}*} - C_9^{\ell\ell'}) \cdot C_{10}^{\ell\ell'*}]$. CP-asymmetries in angular asymmetries, on the other hand, can stem from naïve T -odd observables and do not rely on strong phases ($I_{7,8,9}$). CP-odd ones ($I_{5,6,8,9}$) provide CP-asymmetries that can be measured without tagging, see Ref. [21] for details. A complete and detailed analysis of angular asymmetries in Z' -models is beyond the scope of this work. What we do want to point out here is that a global analysis of angular and CP-asymmetries can probe both $C_9^{\ell\ell'}$ and $C_{10}^{\ell\ell'}$ for electrons, $\ell = e$ and muons, $\ell = \mu$ separately, and therefore can distinguish different $U(1)'$ -charge assignments.

Taking the imaginary part of Eq. (61) and employing Eq. (35), we obtain

$$\text{Im}(C_{9/10}^{\ell\ell'}) \sim \frac{\pi}{\sqrt{2} G_F \alpha_e} \beta_{9/10}^{\ell\ell} \cdot \Delta A_{\text{CP}}^{\text{NP}}, \quad (62)$$

where

$$\beta_{9/10}^{\ell\ell} = \frac{F_{e_i} \pm F_{L_i}}{c_K F_{Q_2} + d_K F_{d_2} - c_\pi F_{Q_1} - d_\pi F_{d_1}}. \quad (63)$$

Values of $\beta_{9/10}^{\ell\ell}$ for $\ell = \mu, e$ in $(\text{TeV})^{-2}$ are given in TABLE III. For $\Delta A_{\text{CP}}^{\text{NP}} \sim 10^{-3}$ we find

$$\text{Im}(C_{9/10}^{\ell\ell'}) \sim 0.03 (\text{TeV})^2 \cdot \beta_{9/10}^{\ell\ell}, \quad (64)$$

consistent with $C_{9/10}^{\ell\ell'} = \mathcal{O}(10^{-2})$ for $g_L^{uc} = 0, g_R^{uc} \neq 0$ [18] and for $\beta_{9/10}^{\ell\ell} = \mathcal{O}(1/\text{TeV}^2)$ (models 2, 4 and 5). Models 9 and 10(μ) have sizable couplings to leptons, and in addition $F_{Q_{1,2}} = 0$, which bring a factor

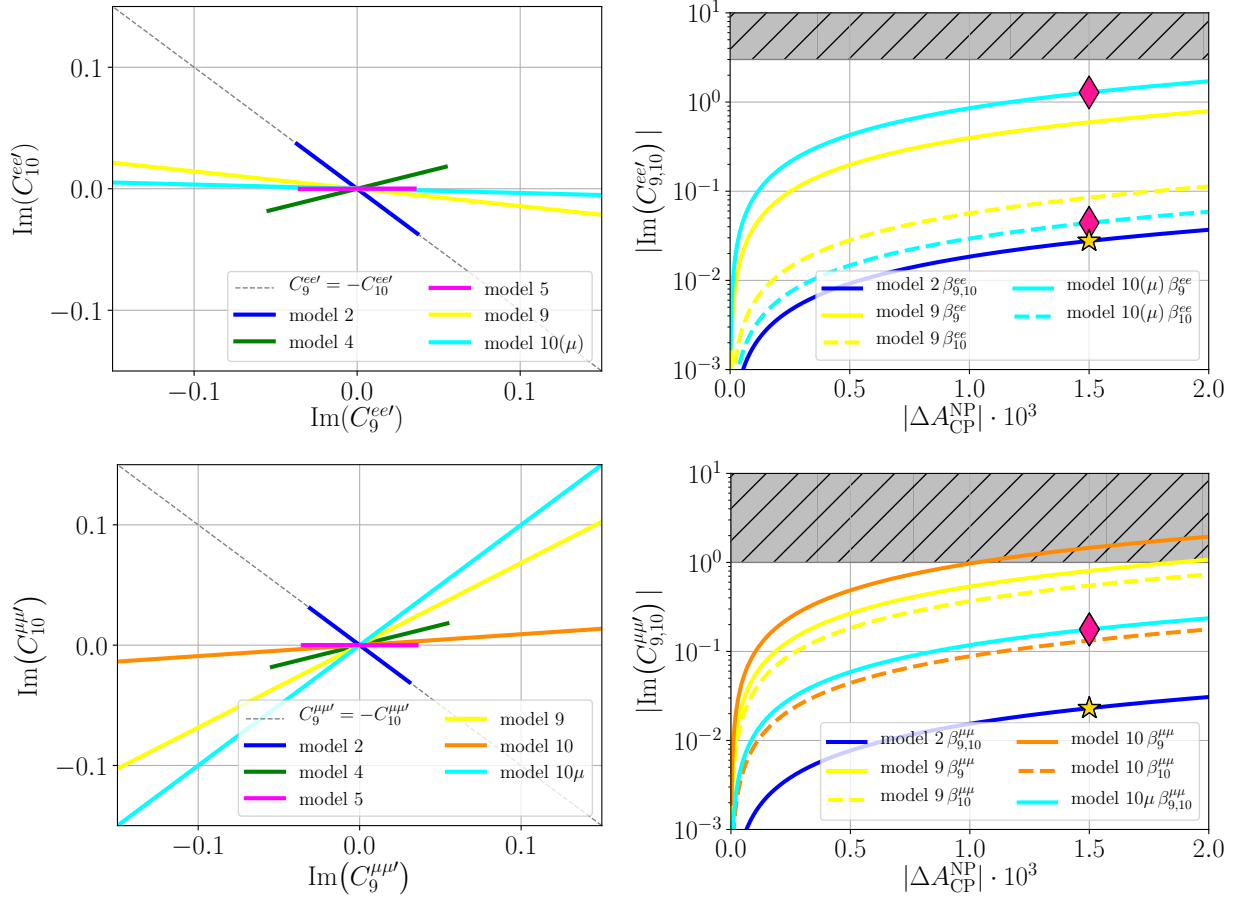


FIG. 5: The interplay between semi-electronic (upper plots) and semi-muonic (lower plots) charm FCNCs (62) and $\Delta A_{\text{CP}}^{\text{NP}}$. The lines for model 2, 4 and 5 end when the corresponding $\Delta A_{\text{CP}}^{\text{NP}}$ exceeds $2 \cdot 10^{-3}$ (plots to the left). In the plots to the right the correlation (62) between $\text{Im}(C_9^{\ell\ell'})$ (solid) and $\text{Im}(C_{10}^{\ell\ell'})$ (dashed) and $|\Delta A_{\text{CP}}^{\text{NP}}|$ in the Z' -models 2, 9, 10 and 10μ is made explicit. The golden star and pink diamond are benchmark points (40) (model 2) and (41) (model 10μ), respectively. The shaded areas correspond to the upper limits (18). See text for details.

of $c_{\pi,K}/d_{\pi,K}$, see Eq. (63), score $\beta_{9/10}^{\ell\ell} = \mathcal{O}(10/\text{TeV}^2)$ and sizable $C_{9/10}^{\ell\ell'} = \mathcal{O}(10^{-1})$. As values of $\text{Im}(C_{9/10}^{\ell\ell'}) \gtrsim \mathcal{O}(10^{-2} - 10^{-1})$ suffice to induce CP-asymmetries beyond the SM in semileptonic D -decays at the few percent level and above [13, 18, 21, 23], all models can simultaneously lead to $\Delta A_{\text{CP}}^{\text{NP}} \sim 10^{-3}$ with NP patterns in $c \rightarrow u \ell^+ \ell^-$ decays.

In FIG. 5 we show the imaginary part of Wilson coefficients with di-electrons (upper plots) and di-muons (lower plots) for different models as in Eq. (62). Plots to the left show lepton vector couplings versus lepton axial vector couplings, $\text{Im}(C_9^{\ell\ell'})$ vs. $\text{Im}(C_{10}^{\ell\ell'})$, respectively. Also given is $\text{Im}(C_{10}^{\ell\ell'}) = -\text{Im}(C_9^{\ell\ell'})$ (thin gray line). The lines corresponding to model 2, 4, and 5 end when the corresponding $\Delta A_{\text{CP}}^{\text{NP}}$ exceeds $2 \cdot 10^{-3}$. Results are lepton non-universal as anticipated and sensitive to the lepton doublet and singlet charges. In the plots to the right the correlation (62) between $\text{Im}(C_9^{\ell\ell'})$ (solid) and $\text{Im}(C_{10}^{\ell\ell'})$ (dashed) and $|\Delta A_{\text{CP}}^{\text{NP}}|$ in the Z' -models 2, 9, 10 and 10μ is made explicit. Curves for models 4 and 5 are only

in mild excess of those for model 2, or smaller, see TABLE III, and are not shown to avoid clutter.

As couplings to electrons and muons differ, lepton non-universality in charm [18, 21, 38] is induced, for example in the ratio of branching ratios of $D \rightarrow \pi \mu^+ \mu^-$ and $D \rightarrow \pi e^+ e^-$ using identical kinematic cuts, R_π^D . To better control SM backgrounds from intermediate resonances $R = \phi, \eta^{(\prime)}, \rho, \dots$, via $D \rightarrow \pi R (\rightarrow \ell^+ \ell^-)$, interesting regions are for low (high) dilepton mass, below the η -mass (above the ϕ -mass), see Ref. [18] for details. We focus on the high mass region as it has fewer sensitivity to unknown strong phases from the resonances.

Using $\beta_{9/10}^{\ell\ell}$ from TABLE III and Eq. (64) we find that all models yield order one deviations from the universality limit $R_\pi^D = 1$. Except for model 10μ , which has smaller couplings to muons by construction, all models can induce significant enhancements or suppressions from the SM. In particular, in the high mass region, for $\phi_R = \pi/2$ and varying strong resonance phases, see Ref. [18] for

details,

$$\begin{aligned} R_\pi^D &\sim [0.6 \dots 1.5] \quad (\text{model 2, 4, 5}) , \\ R_\pi^D &\sim [0.2 \dots 70] \quad (\text{model 9}) , \\ R_\pi^D &\sim [0.2 \dots 11] \quad (\text{model 10}) , \\ R_\pi^D &\sim [0.03 \dots 0.8] \quad (\text{model 10}\mu) , \end{aligned} \quad (65)$$

allowing to signal NP.

VI. CONCLUSIONS

Patterns of observables are indispensable for pinning down an underlying NP-dynamics. We looked globally into hadronic and semileptonic charm decays and their respective CP-asymmetries. We find that there is strong benefit in doing so.

Most important, all flavorful, anomaly-free Z' -models in TABLE I can simultaneously accommodate $\Delta A_{\text{CP}}^{\text{NP}} \sim 10^{-3}$ and induce measurable CP-asymmetries in the semileptonic $c \rightarrow u \ell^+ \ell^-$ modes for $\ell = e$ or $\ell = \mu$ above the SM. An observation of CP-violation in, for instance, $D \rightarrow \pi \ell^+ \ell^-$ or $D \rightarrow \pi \pi \ell^+ \ell^-$ decays supports a NP-interpretation of ΔA_{CP} , Eqs. (1) and (3), see FIG. 5.

Additional cross checks are provided by CP-asymmetries in $D^0 \rightarrow \pi^+ \pi^-$, $D^0 \rightarrow K^+ K^-$, which probe for U-spin breaking NP, see FIGs. 3 and 4 for present data and future sensitivities, respectively. In addition, isospin violating NP can be observed with projected sensitivities at Belle II in $D^0 \rightarrow \pi^0 \pi^0$, $D^+ \rightarrow \pi^+ \pi^0$ decays, whose CP-asymmetries can exceed ΔA_{CP} , Eqs. (54) and (57). In the Z' -models lepton non-universality is generic, and observable in the ratio of branching fractions of $D \rightarrow \pi \mu^+ \mu^-$ and $D \rightarrow \pi e^+ e^-$ decays, as briefly discussed in Section V. The Z' -model 9 with order one enhancements over the universality limit, $R_\pi^D \gg 1$, also induces $A_{\text{CP}}^{\text{NP}}(\pi^+ \pi^0) \sim A_{\text{CP}}^{\text{NP}}(\pi^0 \pi^0) \lesssim 2 \cdot \Delta A_{\text{CP}}^{\text{NP}}$. Z' -model 10 μ with order one suppression of the universality limit, $R_\pi^D < 1$ exhibits sizable NP U-spin breaking $A_{\text{CP}}^{\text{NP}}(\pi^+ \pi^-) \ll A_{\text{CP}}^{\text{NP}}(K^+ K^-) \sim \Delta A_{\text{CP}}$.

Checking correlations pins down models. Improved data and sensitivities from LHCb and Belle II are important in this program. We encourage and look forward to further CP-studies of rare semileptonic and hadronic charm decays.

Acknowledgments

This work is supported by the *Studienstiftung des Deutschen Volkes* (MG) and the *Bundesministerium für Bildung und Forschung – BMBF* (HG).

Appendix A: Experimental input

We extract the modulus of the dominant, SM decay amplitudes from data on branching ratios [27] given in TA-

BLE V. We use

$$\text{BR}(D \rightarrow P_1 P_2) = \frac{|\mathcal{A}_P|^2}{16 \pi m_D} \sqrt{1 - \frac{4m_P^2}{m_D^2}} \tau_D , \quad (\text{A1})$$

where [39]

$$\mathcal{A}_P = \eta_P \lambda_P a_P \frac{G_F}{\sqrt{2}} (m_D^2 - m_P^2) f_0^{D \rightarrow P}(m_P^2) f_P , \quad (\text{A2})$$

$P = \pi, \pi^0, \pi', K$, $\lambda_\pi = \lambda_d$ and $\lambda_K = \lambda_s$ and

$$\eta_P = \begin{cases} 1 & P = \pi, \pi^0, K \\ \frac{1}{\sqrt{2}} & P = \pi' \end{cases} . \quad (\text{A3})$$

The subscript π' corresponds to the $D^+ \rightarrow \pi^+ \pi^0$ channel, and π^0 to $D^0 \rightarrow \pi^0 \pi^0$. Relevant form factors $f_0^{D \rightarrow P}$ and decay constants f_P are taken from Ref. [40] and [27], respectively. Resulting values of $a_P > 0$ are given in TABLE V.

mode	BR(mode)	a_P
$D^0 \rightarrow K^+ K^-$	$(4.08 \pm 0.06) \cdot 10^{-3}$	1.19 ± 0.04
$D^0 \rightarrow \pi^+ \pi^-$	$(1.455 \pm 0.024) \cdot 10^{-3}$	0.94 ± 0.07
$D^0 \rightarrow \pi^0 \pi^0$	$(8.26 \pm 0.25) \cdot 10^{-4}$	0.71 ± 0.05
$D^+ \rightarrow \pi^0 \pi^+$	$(1.247 \pm 0.033) \cdot 10^{-3}$	0.77 ± 0.05

TABLE V: Measured branching ratios [27] and a_P -parameters from Eq. (A2) for different decay modes.

Appendix B: Evolution of Wilson coefficients

The Wilson coefficients $\tilde{C}_{7,8,9,10}^{(\prime)}$ at the Z' mass scale (32) are evolved to the charm mass scale at LO in α_s . The requisite anomalous dimension matrix for the operators $\tilde{Q}_{7,8,9,10}$ can be inferred from Ref. [41]. We obtain

$$\gamma_F^0 = \begin{pmatrix} \frac{6}{N_C} & -6 & 0 & 0 \\ 0 & \frac{6(1-N_C^2)}{N_C} & 0 & 0 \\ 0 & 0 & \frac{-6}{N_C} & 6 \\ 0 & 0 & 6 & \frac{-6}{N_C} \end{pmatrix} , \quad (\text{B1})$$

where $N_C = 3$ is the number of colors. Since QCD conserves parity, γ_F^0 is identical for \tilde{Q}_i and \tilde{Q}'_i . Using Eq. (B1), the Wilson coefficients are evolved to the charm scale, integrating out degrees of freedom at the (Z', t, b) -scales,

$$\vec{C}(\mu) = U_4(\mu, m_b) \hat{U}_5(m_b, m_t) \hat{U}_6(m_t, M_{Z'}) \vec{C}(M_{Z'}) ,$$

where $\hat{U}_f(m_1, m_2) \equiv M_f(m_1) U_f(m_1, m_2)$ and $U_f(m_1, m_2)$ is the evolution matrix from scale m_2 to scale m_1 in an effective field theory with f active

flavors; M_f is the threshold matrix that matches the two effective theories with $f - 1$ and f active flavors. At LO in α_s , the M_f matrices are equal to the identity matrix. For $\mu = m_c$ and $M_{Z'} = 6 \text{ TeV}$, one finds

$$\begin{aligned}\tilde{C}_7^{(l)}(m_c) &= 0.829 \tilde{C}_7^{(l)}(M_{Z'}) , \\ \tilde{C}_8^{(l)}(m_c) &= 1.224 \tilde{C}_7^{(l)}(M_{Z'}) + 4.502 \tilde{C}_8^{(l)}(M_{Z'}) , \\ \tilde{C}_9^{(l)}(m_c) &= 1.404 \tilde{C}_9^{(l)}(M_{Z'}) - 0.718 \tilde{C}_{10}^{(l)}(M_{Z'}) , \\ \tilde{C}_{10}^{(l)}(m_c) &= -0.718 \tilde{C}_9^{(l)}(M_{Z'}) + 1.404 \tilde{C}_{10}^{(l)}(M_{Z'}) .\end{aligned}\quad (\text{B2})$$

We use $m_c = (1.280 \pm 0.013) \text{ GeV}$, $m_b = (4.198 \pm 0.012) \text{ GeV}$ [42] and $m_t = (165.9 \pm 2.1) \text{ GeV}$ [43, 44] and central values for the thresholds.

Appendix C: Hadronic matrix elements

In order to estimate the NP decay amplitudes, we need to determine the hadronic matrix elements for each operator given by Eqs. (24)–(31). For that purpose, we employ factorization of currents, $P = \pi, K$,

$$\begin{aligned}\langle P^+ P^- | Q_i | D^0 \rangle & \quad (\text{C1}) \\ = \langle P^+ | (\bar{q}_1 \Gamma_1 q_2) | 0 \rangle \langle P^- | (\bar{q}_3 \Gamma_2 q_4) | D^0 \rangle B_i^{P^+ P^-} ,\end{aligned}$$

where $Q_i = (\bar{q}_1 \Gamma_1 q_2) (\bar{q}_3 \Gamma_2 q_4)$ is a 4-quark operator and $\Gamma_{1,2}$ represent possible Dirac and color structures while q_j denote quarks. The factor $B_i^{P^+ P^-}$ parametrizes the deviation of the true hadronic matrix element from its naïve approximation, $B_i^{P^+ P^-}|_{\text{naïve}} = 1$. For the NP contributions we work in this approximation. After employing Fierz identities in the flavor and color space, we find for $D^0 \rightarrow K^+ K^-$ and $\pi^+ \pi^-$ decays

$$\langle \tilde{Q}_7 \rangle_{K,\pi} = \frac{1}{N_C} \langle \tilde{Q}_8 \rangle_{K,\pi} , \quad (\text{C2})$$

$$\langle \tilde{Q}_8 \rangle_{K,\pi} = F_{d_2, d_1} \chi_{K,\pi}(\mu) \langle Q_1^{s,d} \rangle_{K,\pi} , \quad (\text{C3})$$

$$\langle \tilde{Q}_9 \rangle_{K,\pi} = \frac{1}{N_C} \langle \tilde{Q}_{10} \rangle_{K,\pi} , \quad (\text{C4})$$

$$\langle \tilde{Q}_{10} \rangle_{K,\pi} = F_{Q_2, Q_1} \langle Q_1^{s,d} \rangle_{K,\pi} , \quad (\text{C5})$$

where $\langle \dots \rangle_P = \langle P^+ P^- | \dots | D^0 \rangle$, $Q_1^p = (\bar{u}p)_{V-A} (\bar{p}c)_{V-A}$ and $\chi_{K,\pi}(\mu)$ are the usual chiral enhancements generated by $(V-A) \times (V+A)$ operators,

$$\begin{aligned}\chi_K(\mu) &= \frac{2 M_K^2}{m_c(\mu) m_s(\mu)} , \\ \chi_\pi(\mu) &= \frac{2 M_\pi^2}{m_c(\mu) (m_d + m_u)(\mu)} ,\end{aligned}\quad (\text{C6})$$

with values $\chi_K(m_c) \approx 3.626$ and $\chi_\pi(m_c) \approx 3.655$ at the charm mass scale. For the \tilde{Q}'_i operators the same relations hold but with the proper exchange of charges $F_{Q_i} \leftrightarrow F_{d_i}$.

For $D^+ \rightarrow \pi^0 \pi^+$ decays we find

$$\langle \tilde{Q}_7 \rangle_{\pi'} = \frac{1}{N_C} \langle \tilde{Q}_8 \rangle_{\pi'} , \quad (\text{C7})$$

$$\langle \tilde{Q}_8 \rangle_{\pi'} = \frac{\chi_\pi(\mu)}{\sqrt{2}} (F_{u_1} - F_{d_1}) \langle Q_1^u \rangle_u , \quad (\text{C8})$$

$$\langle \tilde{Q}_9 \rangle_{\pi'} = \frac{1}{N_C} \langle \tilde{Q}_{10} \rangle_{\pi'} = 0 , \quad (\text{C9})$$

and for the corresponding \tilde{Q}'_i operators

$$\langle \tilde{Q}'_7 \rangle_{\pi'} = \frac{1}{N_C} \langle \tilde{Q}'_8 \rangle_{\pi'} = 0 , \quad (\text{C10})$$

$$\langle \tilde{Q}'_9 \rangle_{\pi'} = \frac{1}{N_C} \langle \tilde{Q}'_{10} \rangle_{\pi'} , \quad (\text{C11})$$

$$\langle \tilde{Q}'_{10} \rangle_{\pi'} = \frac{1}{\sqrt{2}} (F_{u_1} - F_{d_1}) \langle Q_1^u \rangle_u . \quad (\text{C12})$$

For $D^0 \rightarrow \pi^0 \pi^0$ decays we obtain

$$\langle \tilde{Q}_7 \rangle_{\pi^0} = \frac{1}{N_C} \langle \tilde{Q}_8 \rangle_{\pi^0} , \quad (\text{C13})$$

$$\langle \tilde{Q}_8 \rangle_{\pi^0} = \frac{\chi_\pi(\mu)}{2} (F_{u_1} - F_{d_1}) \langle Q_1^u \rangle_u , \quad (\text{C14})$$

$$\langle \tilde{Q}_9 \rangle_{\pi^0} = \frac{1}{N_C} \langle \tilde{Q}_{10} \rangle_{\pi^0} = 0 , \quad (\text{C15})$$

and for the corresponding \tilde{Q}'_i operators

$$\langle \tilde{Q}'_7 \rangle_{\pi^0} = \frac{1}{N_C} \langle \tilde{Q}'_8 \rangle_{\pi^0} = 0 , \quad (\text{C16})$$

$$\langle \tilde{Q}'_9 \rangle_{\pi^0} = \frac{1}{N_C} \langle \tilde{Q}'_{10} \rangle_{\pi^0} , \quad (\text{C17})$$

$$\langle \tilde{Q}'_{10} \rangle_{\pi^0} = \frac{1}{2} (F_{u_1} - F_{d_1}) \langle Q_1^u \rangle_u , \quad (\text{C18})$$

where $\langle \dots \rangle_{\pi'} = \langle \pi^+ \pi^0 | \dots | D^+ \rangle$, $\langle \dots \rangle_{\pi^0} = \langle \pi^0 \pi^0 | \dots | D^0 \rangle$ and $\langle \dots \rangle_q = \langle \bar{q}q | \dots | D^+ \rangle$. Eqs. (C2)–(C18) are obtained in the isospin limit, $m_u = m_d$ and $e = 0$, since these isospin breaking corrections from within the SM are negligible with respect to the NP ones, $F_{u_i, d_i, Q_i} \neq 0$.

Appendix D: RGE functions

Eq. (35) for $\Delta A_{\text{CP}}^{\text{NP}}$ accounts for the running and mixing of operators through the functions $r_{1,2}$. The latter can be obtained from the evolution of the Wilson coefficients described in Appendix B. We obtain

$$r_1(m_c, M_{Z'}) = \frac{R^{-2}}{3 \sqrt{2} G_F \lambda_s} , \quad (\text{D1})$$

$$r_2(m_c, M_{Z'}) = \frac{2 R^{1/2} - R^{-1}}{3 \sqrt{2} G_F \lambda_s} , \quad (\text{D2})$$

where

$$R = \left(\frac{\alpha_s^{(4)}(m_b)}{\alpha_s^{(4)}(m_c)} \right)^{\frac{12}{25}} \left(\frac{\alpha_s^{(5)}(m_t)}{\alpha_s^{(5)}(m_b)} \right)^{\frac{12}{23}} \left(\frac{\alpha_s^{(6)}(M_{Z'})}{\alpha_s^{(6)}(m_t)} \right)^{\frac{4}{7}} . \quad (\text{D3})$$

-
- [1] R. Aaij *et al.* [LHCb Collaboration], Phys. Rev. Lett. **122**, no. 21, 211803 (2019) doi:10.1103/PhysRevLett.122.211803 [arXiv:1903.08726 [hep-ex]].
- [2] Y. S. Amhis *et al.* [HFLAV Collaboration], arXiv:1909.12524 [hep-ex].
- [3] M. Chala, A. Lenz, A. V. Rusov and J. Scholtz, JHEP **1907**, 161 (2019) doi:10.1007/JHEP07(2019)161 [arXiv:1903.10490 [hep-ph]].
- [4] A. Dery and Y. Nir, JHEP **1912**, 104 (2019) doi:10.1007/JHEP12(2019)104 [arXiv:1909.11242 [hep-ph]].
- [5] F. Buccella, A. Paul and P. Santorelli, Phys. Rev. D **99** (2019) no.11, 113001 doi:10.1103/PhysRevD.99.113001 [arXiv:1902.05564 [hep-ph]].
- [6] H. N. Li, C. D. Lü and F. S. Yu, arXiv:1903.10638 [hep-ph].
- [7] A. Soni, arXiv:1905.00907 [hep-ph].
- [8] H. Y. Cheng and C. W. Chiang, Phys. Rev. D **100** (2019) no.9, 093002 doi:10.1103/PhysRevD.100.093002 [arXiv:1909.03063 [hep-ph]].
- [9] A. Khodjamirian and A. A. Petrov, Phys. Lett. B **774** (2017) 235 doi:10.1016/j.physletb.2017.09.070 [arXiv:1706.07780 [hep-ph]].
- [10] A. L. Kagan and L. Silvestrini, arXiv:2001.07207 [hep-ph].
- [11] U. Nierste, arXiv:2002.06686 [hep-ph].
- [12] A. Pich, PoS LHCP **2019** (2019) 078 doi:10.22323/1.350.0078 [arXiv:1911.06211 [hep-ph]].
- [13] S. Fajfer and N. Košnik, Phys. Rev. D **87**, no. 5, 054026 (2013) doi:10.1103/PhysRevD.87.054026 [arXiv:1208.0759 [hep-ph]].
- [14] J. Ellis, M. Fairbairn and P. Tunney, Eur. Phys. J. C **78** (2018) no.3, 238 doi:10.1140/epjc/s10052-018-5725-0 [arXiv:1705.03447 [hep-ph]].
- [15] B. C. Allanach, J. Davighi and S. Melville, JHEP **1902** (2019) 082 doi:10.1007/JHEP02(2019)082 [arXiv:1812.04602 [hep-ph]].
- [16] J. Rathsman and F. Tellander, arXiv:1902.08529 [hep-ph].
- [17] D. B. Costa, B. A. Dobrescu and P. J. Fox, arXiv:1905.13729 [hep-th].
- [18] R. Bause, M. Golz, G. Hiller and A. Tayduganov, Eur. Phys. J. C **80**, no. 1, 65 (2020) doi:10.1140/epjc/s10052-020-7621-7 [arXiv:1909.11108 [hep-ph]].
- [19] J. Aebischer, A. J. Buras, M. Cerdà-Sevilla and F. De Fazio, JHEP **2002** (2020) 183 doi:10.1007/JHEP02(2020)183 [arXiv:1912.09308 [hep-ph]].
- [20] D. Choudhury, K. Deka, T. Mandal and S. Sadhukhan, arXiv:2002.02349 [hep-ph].
- [21] S. De Boer and G. Hiller, Phys. Rev. D **98**, no. 3, 035041 (2018) doi:10.1103/PhysRevD.98.035041 [arXiv:1805.08516 [hep-ph]].
- [22] R. Aaij *et al.* [LHCb Collaboration], Phys. Rev. Lett. **121** (2018) no.9, 091801 doi:10.1103/PhysRevLett.121.091801 [arXiv:1806.10793 [hep-ex]].
- [23] S. de Boer and G. Hiller, Phys. Rev. D **93**, no. 7, 074001 (2016) doi:10.1103/PhysRevD.93.074001 [arXiv:1510.00311 [hep-ph]].
- [24] J. Fuentes-Martin, A. Greljo, J. Martin Camalich and J. D. Ruiz-Alvarez, [arXiv:2003.12421 [hep-ph]].
- [25] B. Holdom, Phys. Lett. **166B** (1986) 196. doi:10.1016/0370-2693(86)91377-8
- [26] W. Altmannshofer, R. Primulando, C. T. Yu and F. Yu, JHEP **1204** (2012) 049 doi:10.1007/JHEP04(2012)049 [arXiv:1202.2866 [hep-ph]].
- [27] M. Tanabashi *et al.* [Particle Data Group], Phys. Rev. D **98** (2018) no.3, 030001.
- [28] Y. Grossman, Z. Ligeti and D. J. Robinson, JHEP **1401** (2014) 066 doi:10.1007/JHEP01(2014)066 [arXiv:1308.4143 [hep-ph]].
- [29] Y. Grossman and S. Schacht, JHEP **1907** (2019) 020 doi:10.1007/JHEP07(2019)020 [arXiv:1903.10952 [hep-ph]].
- [30] Y. Grossman and S. Schacht, Phys. Rev. D **99**, no. 3, 033005 (2019) doi:10.1103/PhysRevD.99.033005 [arXiv:1811.11188 [hep-ph]].
- [31] S. Müller, U. Nierste and S. Schacht, Phys. Rev. Lett. **115** (2015) no.25, 251802 doi:10.1103/PhysRevLett.115.251802 [arXiv:1506.04121 [hep-ph]].
- [32] H. Mendez *et al.* [CLEO Collaboration], Phys. Rev. D **81** (2010) 052013 doi:10.1103/PhysRevD.81.052013 [arXiv:0906.3198 [hep-ex]].
- [33] R. Aaij *et al.* [LHCb Collaboration], arXiv:1808.08865.
- [34] E. Kou *et al.* [Belle-II Collaboration], PTEP **2019**, no. 12, 123C01 (2019) doi:10.1093/ptep/ptz106 [arXiv:1808.10567 [hep-ex]].
- [35] Y. Grossman, A. L. Kagan and J. Zupan, Phys. Rev. D **85** (2012) 114036 doi:10.1103/PhysRevD.85.114036 [arXiv:1204.3557 [hep-ph]].
- [36] G. Hiller, M. Jung and S. Schacht, Phys. Rev. D **87**, no. 1, 014024 (2013) doi:10.1103/PhysRevD.87.014024 [arXiv:1211.3734 [hep-ph]].
- [37] L. Cappiello, O. Cata and G. D'Ambrosio, JHEP **04** (2013), 135 doi:10.1007/JHEP04(2013)135 [arXiv:1209.4235 [hep-ph]].
- [38] S. Fajfer and N. Košnik, Eur. Phys. J. C **75** (2015) no.12, 567 doi:10.1140/epjc/s10052-015-3801-2 [arXiv:1510.00965 [hep-ph]].
- [39] Y. Grossman, A. L. Kagan and Y. Nir, Phys. Rev. D **75** (2007) 036008 [hep-ph/0609178].
- [40] V. Lubicz *et al.* [ETM Collaboration], Phys. Rev. D **96** (2017) no.5, 054514 Erratum: [Phys. Rev. D **99** (2019) no.9, 099902] doi:10.1103/PhysRevD.96.054514, 10.1103/PhysRevD.99.099902 [arXiv:1706.03017 [hep-lat]].
- [41] G. Buchalla, A. J. Buras and M. E. Lautenbacher, Rev. Mod. Phys. **68** (1996) 1125 doi:10.1103/RevModPhys.68.1125 [hep-ph/9512380].
- [42] S. Aoki *et al.* [Flavour Lattice Averaging Group], Eur. Phys. J. C **80** (2020) no.2, 113 doi:10.1140/epjc/s10052-019-7354-7 [arXiv:1902.08191 [hep-lat]].
- [43] J. Fuster, A. Irles, D. Melini, P. Uwer and M. Vos, Eur. Phys. J. C **77** (2017) no.11, 794 doi:10.1140/epjc/s10052-017-5354-z [arXiv:1704.00540 [hep-ph]].
- [44] G. Aad *et al.* [ATLAS Collaboration], JHEP **1510** (2015) 121 doi:10.1007/JHEP10(2015)121 [arXiv:1507.01769 [hep-ex]].